The 9th European Congress on Computational Methods in Applied Sciences and Engineering
ECCOMAS Congress 2024
3–7 June 2024, Lisboa, Portugal

ANALYSIS OF TURBULENT FLOWS VIA ROBUST SPECTRAL PROPER ORTHOGONAL DECOMPOSITION

Antonio Colanera[1], Oliver T. Schmidt[2] and Matteo Chiatto[1]

[1] Department of Industrial Engineering,
Università degli Studi di Napoli "Federico II",
Naples (80125), Italy
e-mail: antonio.colanera@unina.it

[2] Department of Mechanical and Aerospace Engineering,
University of California San Diego,
La Jolla, San Diego (CA 92161), United States

Key words: Low-dimensional models; modal analysis, turbulent flows

Summary. In many experimental measurements, corrupted data and outliers can significantly distort the coherent structures identified through traditional modal analysis techniques. This distortion becomes particularly pronounced at higher frequencies, where the corresponding modes are more susceptible to contamination from measurement noise and uncertainties. To address these limitations, we introduce a novel approach, robust spectral proper orthogonal decomposition (robust SPOD), which incorporates the robust principal component analysis method into the SPOD. In this work, we assess robust SPOD effectiveness through applications to two distinct fluid dynamics problems: a numerically simulated turbulent subsonic jet flow field and experimental data of the flow within an open cavity. When applied to turbulent jet data artificially corrupted by salt and pepper and Gaussian noise, the robust SPOD produces more converged and physically interpretable modes than the standard SPOD method. Furthermore, we illustrate how robust SPOD can be employed as a powerful tool for data denoising, relying on signal reconstruction from denoised modes. The analysis of the open cavity flow with the robust SPOD yields smoother spatial distributions of modes, particularly at high frequencies and for higher-order modes when compared to the conventional SPOD approach.

1 INTRODUCTION

Data corruption presents a significant challenge in systems modeling and forecasting, where noisy and incomplete measurements can severely compromise the integrity of learned models and lead to erroneous conclusions. Effectively managing such data is crucial for the development of reduced-order models (ROMs) and for deriving physical insights from experimental studies.

A commonly employed approach to constructing a ROM involves extracting physically significant features or modes that characterize the flow topology and projecting the Navier-Stokes equations onto a subset of these modes via Galerkin projection, resulting in a system of ordinary differential equations [1]. By selecting a limited set of modes, it becomes feasible to develop a reduced model that can predict the flow behavior with lower computational costs. Various techniques are available for identifying the primary coherent structures of the flow [2, 3], although these methods can be sensitive to the presence of outliers and incomplete data.

Among the modal analysis techniques, spectral proper orthogonal decomposition (SPOD) has garnered substantial attention in recent years due to its ability to extract the dominant spectral features of a flow field. SPOD optimally captures two-point space–time correlations, yielding modes that evolve coherently in both space and time [4, 5, 6]. This algorithm has been widely applied in fluid dynamics, primarily for the post-processing of numerical and experimental data. It serves as a powerful tool for investigating flow topology [7, 8, 9, 10, 11] and for evaluating flow receptivity and the efficacy of control strategies [12].

Particle image velocimetry (PIV) is one of the most prevalent experimental measurement techniques used today. However, PIV data can suffer from errors caused by inadequate illumination, optical issues, reflections, and sharp gradients in field properties [13]. Experimental measurements must navigate a trade-off between the quantity and quality of PIV data, often resulting in flow fields that contain corrupt or missing measurements. Standard filtering and reconstruction techniques typically involve interpolation methods that rely solely on local flow information [14], as well as least-squares methods and Kriging [15].

The challenge of incomplete measurements has traditionally been addressed using approaches based on proper orthogonal decomposition (POD), as explored in works such as [16], [17], and [18]. More recently, [19] demonstrated the effectiveness of gappy SPOD in reconstructing flow fields. Additionally, machine learning techniques, including Physics-informed neural networks (PINNs) [20], long short-term memory (LSTM) networks [21], deep generative adversarial networks (GANs) [22], and autoencoders [23], have shown promise in generating missing data in turbulence and processing PIV data.

Conversely, the issue of outliers, particularly when their locations are unknown, has been effectively addressed using matrix completion techniques. These methods separate sparse noise from the data [24] through various algorithmic approaches, such as the augmented Lagrange multiplier (ALM) method and the alternating directions method (ADM) [25, 26]. These techniques have proven valuable for the post-processing of experimental data and in modal decompositions [27].

The SPOD technique's algorithm represents a frequency-domain extension of the standard space-only POD [28], which is not robust against outliers and corrupted data. This work aims to address this limitation by introducing the robust spectral proper orthogonal decomposition (robust SPOD) and providing a detailed description of its algorithm. The technique is applied to classical fluid dynamics problems to analyze various aspects of the algorithm, including the subsonic jet flow field numerically computed using large-eddy simulations (LES) from [4] and the flow within an open cavity, obtained from PIV measurements in [29].

The remainder of this paper is structured as follows. Section 2 introduces the robust SPOD procedure. The results are presented in Section 3.

2 ROBUST SPOD

Consider a snapshot ensemble $\{\boldsymbol{q}_i\}$, representing a collection of instantaneous states of a generic field $\boldsymbol{q}(\boldsymbol{x}, t)$, defined over the spatial domain $\boldsymbol{x}$ at discrete times t_i (with $i = 1, \ldots, M$). These snapshots are arranged to form a data matrix $\boldsymbol{Q} \in \mathbb{R}^{N \times M}$, where N represents the total length of the state vector, corresponding to the number of grid points multiplied by the number of flow variables. The data matrix $\boldsymbol{Q}$ is further divided into N_b blocks, denoted by $\mathbf{Q}^{(j)}$, with j ranging from 1 to N_b. Each block consists of N_f snapshots, which may overlap with one another; the number of overlapping snapshots is denoted as N_o. For each block, a (windowed) discrete Fourier transform (FFT) is computed, and the Fourier components for each block are then stacked into a matrix $\hat{\mathbf{Q}}_{f_k} \in \mathbb{R}^{N \times N_b}$ for each frequency f_k, with $k = 1, \ldots, N_f$.

The standard SPOD algorithm, as detailed in [5] and [30], relies on the eigenvalue decomposition of the cross-spectral density (CSD) matrix, defined as:

$$\mathbf{S}_{f_k} = \hat{\mathbf{Q}}_{f_k} \hat{\mathbf{Q}}_{f_k}^* \boldsymbol{W}, \tag{1}$$

where $\boldsymbol{W}$ is a spatial weight matrix that accounts for the non-uniformity of the data, as described in [31]. If the original data contain outliers, these anomalies are likely to persist (and possibly be amplified) in the Fourier realizations, leading to corrupted and noisy modes. To mitigate this issue, we propose integrating robust principal component analysis (PCA) within the SPOD framework, as introduced by [24] and reviewed by [27].

Robust PCA decomposes the matrix of Fourier realizations $\hat{\mathbf{Q}}_{f_k}$ (or equivalently, the snapshot blocks $\mathbf{Q}^{(j)}$) into:

$$\hat{\mathbf{Q}}_{f_k} = \hat{\mathbf{L}}_{f_k} + \hat{\mathbf{H}}_{f_k}, \tag{2}$$

where $\hat{\mathbf{L}}_{f_k}$ represents a low-rank structure, and $\hat{\mathbf{H}}_{f_k}$ is a sparse matrix containing outliers and corrupted data [24]. Consequently, the principal components of $\hat{\mathbf{L}}_{f_k}$ remain unaffected by erroneous data.

To demonstrate how robust PCA isolates outliers in the matrix $\hat{\mathbf{H}}_{f_k}$, consider that for standard POD, the mathematical formulation for extracting the desired low-rank structures $\hat{\mathbf{L}}_{f_k}$ involves minimizing the Frobenius norm ($\|\cdot\|_F$) of the term $\hat{\mathbf{H}}_{f_k} = \hat{\mathbf{Q}}_{f_k} - \hat{\mathbf{L}}_{f_k}$:

$$\min_{\hat{\mathbf{L}}_{f_k}} \|\hat{\mathbf{Q}}_{f_k} - \hat{\mathbf{L}}_{f_k}\|_F \quad \text{subject to} \quad \text{rank}(\hat{\mathbf{L}}_{f_k}) \leq r. \tag{3}$$

The use of the Frobenius norm renders the computation highly sensitive to outliers.

In contrast, the robust PCA formulation involves the following optimization problem:

$$\min_{\hat{\mathbf{L}}_{f_k}, \hat{\mathbf{H}}_{f_k}} \text{rank}(\hat{\mathbf{L}}_{f_k}) + \|\hat{\mathbf{H}}_{f_k}\|_0 \quad \text{subject to} \quad \hat{\mathbf{L}}_{f_k} + \hat{\mathbf{H}}_{f_k} = \hat{\mathbf{Q}}_{f_k}, \tag{4}$$

where $\|\hat{\mathbf{H}}_{f_k}\|_0$ represents the cardinality of the nonzero elements in $\hat{\mathbf{H}}_{f_k}$, indicating the sparsity of $\hat{\mathbf{H}}_{f_k}$. This problem (4) is non-convex and is typically solved by considering its convex relaxation [24]:

$$\min_{\hat{\mathbf{L}}_{f_k}, \hat{\mathbf{H}}_{f_k}} \|\hat{\mathbf{L}}_{f_k}\|_* + \alpha_0 \|\hat{\mathbf{H}}_{f_k}\|_1 \quad \text{subject to} \quad \hat{\mathbf{L}}_{f_k} + \hat{\mathbf{H}}_{f_k} = \hat{\mathbf{Q}}_{f_k}, \tag{5}$$

where $\|\cdot\|_*$ denotes the nuclear norm (sum of singular values), and $\|\cdot\|_1$ represents the L_1 norm (sum of the magnitudes of each entry in the matrix). The coefficient α_0 is defined as:

$$\alpha_0 = \alpha / \sqrt{\max(N, N_b)}, \tag{6}$$

where α is a tunable parameter representing the filter intensity [27].

The problem (5) is known as *principal component pursuit* and can be solved using the augmented Lagrange multiplier (ALM) algorithm, as discussed in [26] and [25]. Following [24], the augmented Lagrangian is defined as:

$$\ell(\hat{\mathbf{L}}_{f_k}, \hat{\mathbf{H}}_{f_k}, \mathbf{Y}) = \|\hat{\mathbf{L}}_{f_k}\|_* + \alpha_0 \|\hat{\mathbf{H}}_{f_k}\|_1 + \langle \mathbf{Y}, \hat{\mathbf{Q}}_{f_k} - \hat{\mathbf{L}}_{f_k} - \hat{\mathbf{H}}_{f_k} \rangle + \frac{\mu}{2} \|\hat{\mathbf{Q}}_{f_k} - \hat{\mathbf{L}}_{f_k} - \hat{\mathbf{H}}_{f_k}\|_F^2, \tag{7}$$

where $\mathbf{Y}$ is the matrix of Lagrange multipliers, $\langle \cdot, \cdot \rangle$ denotes the standard trace inner product, and μ is a parameter that quantifies the error in (2). In this work, μ is chosen according to $\mu = 0.25 N N_b / \|\hat{\mathbf{Q}}_{f_k}\|_1$.

Notably, μ does not affect the solution of problem (4) but influences the convergence speed. The optimal set of $(\hat{\mathbf{L}}_{f_k}, \hat{\mathbf{H}}_{f_k}, \mathbf{Y})$ that minimizes (7) can be found using various methods, as detailed in [24], [26], and [25]. In this study, the alternating directions method (ADM) has been employed. Once the robust PCA algorithm converges, the resulting de-noised Fourier realizations matrix $\hat{\mathbf{L}}_{f_k}$ is utilized in the standard SPOD procedure in place of $\hat{\mathbf{Q}}_{f_k}$.

Further details on the algorithm and hyperparameter tuning can be found in [32].

3 Results

Our investigation focuses on the flow field within an open cavity, where measurements were acquired using a time-resolved PIV technique. The standard SPOD tends to produce noisy results, especially for non-leading modes. As demonstrated in this paper, the application of robust SPOD enhances the smoothness and physical interpretability of these modes. The dataset reported in [29] was considered here, specifically for a free stream Mach number (defined as the ratio between the incoming flow velocity U_c and the speed of sound a_c) equal to $M = 0.6$.

Panel (a) of Figure 1 shows a sketch of the rectangular cavity. The cavity has a length of $L_c = 158.8$ mm, a depth of $D_c = 26.4$ mm, and a width of $W_c = 101.6$ mm, resulting in nondimensional ratios of $L_c/D_c = 6$ and $W_c/D_c = 3.85$.

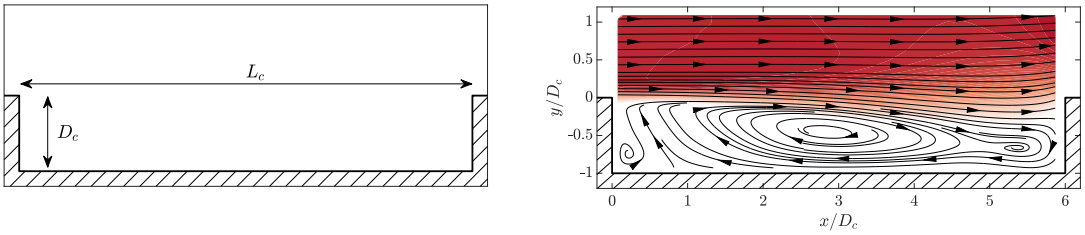

(a) (b)

Figure 1: Open cavity flows. Panel (a): geometrical sketch; panel (b): mean streamwise velocity component and streamlines distribution. Data courtesy of [29].

As depicted in panel (b) of Figure 1, which illustrates the temporal mean distribution of the streamwise velocity component, the incoming boundary layer separates at the leading edge of the cavity, forming a shear layer. This shear layer is convectively unstable, leading to the generation of Kelvin-Helmholtz instability waves. These waves travel downstream, impinge on the back edge of the cavity, and partially reflect as acoustic waves. Then, they propagate upstream and lock in with the Kelvin-Helmholtz instability at the leading edge, completing a feedback cycle [29, 33, 34]. This feedback process results in an aeroacoustic resonance whose main tones are known as Rossiter modes [35]. The characteristic dimensionless frequencies (in terms of the Strouhal number, St) associated with these modes can be predicted using the empirical relation:

$$St_n = \frac{f_n L_c}{U_\infty} = \frac{n - a}{1/\kappa_r + M/\sqrt{1 + (\gamma - 1)M^2/2}}. \tag{8}$$

Here, U_∞ represents the freestream velocity, $\kappa_r = 0.65$ is an empirical coefficient, $a = 0.38$ is the phase lag, and $n = 1, 2, \ldots$ corresponds to the Rossiter mode index. Equation (8) predicts the dimensionless frequencies St_n associated with the resonance modes in open cavities.

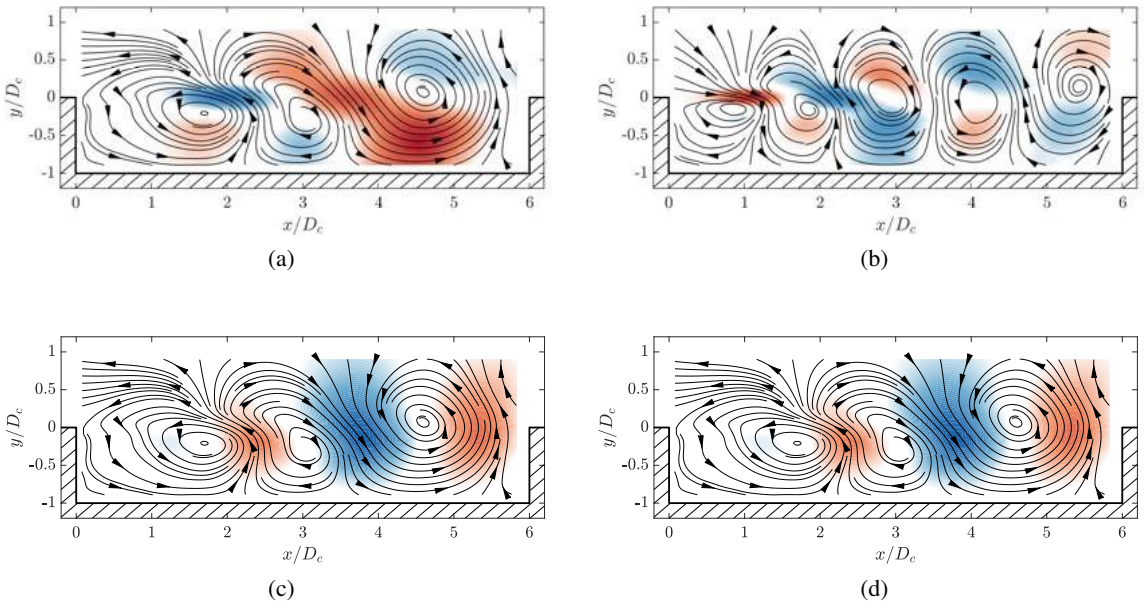

Figure 2: Leading SPOD modes of open cavity flows data from [29]. Panel (a): real part of leading SPOD mode of u at $St = 0.75$. Panel (b): real part of leading SPOD mode of u at $St = 1.22$. Panel (c): real part of leading SPOD mode of v at $St = 0.75$. Panel (d): real part of leading SPOD mode of v at $St = 1.22$.

Velocity components were measured on a uniform grid with dimensions $n_x \times n_y = 156 \times 55$ and with a sampling frequency of $f_s = 16000$ Hz. The analysis is based on $N_t = 16000$ snapshots, with $N_b = 30$ blocks and $N_f = 1024$ frequencies. Figure 2 presents the real part of the first SPOD mode at the two leading frequencies, $St = 0.75$ and $St = 1.22$. Panels (a) and (b) show the streamwise component of the mode, while panels (c) and (d) show the transverse component. The spatial structures at higher frequencies exhibit finer scales than those at lower frequencies.

For this case, the robust SPOD analysis is performed with a de-noising parameter $\alpha = 1$. Figure 3 presents the spectra obtained from both SPOD (black lines) and robust SPOD (blue lines) analysis. The robust SPOD analysis primarily focuses on reducing noise at high frequencies, meaning that the reconstructed signals exhibit less noise contamination than those obtained from SPOD, particularly in the higher frequency range. To provide a reference for the spectral behavior, the red dashed line represents the Kolmogorov power law ($St^{-5/3}$), which is a well-established representation of the energy spectrum in turbulent flows and serves as a benchmark for assessing the spectral characteristics of the analyzed data, showing how the curve tends to align with this well-known benchmark. As expected, the power law scaling is not valid at low frequencies, where relatively larger coherent structures characterize the flow.

Figure 4 compares the leading v modes obtained from both SPOD and robust SPOD analysis. The comparison is made for the first four Rossiter frequencies and a generic high Strouhal number ($St = 4$).

It is worth noting that applying robust SPOD leads to considerable improvements in the smoothness of the extracted modes. Specifically, SPOD already performs well for the first mode at the leading frequencies ($St = 0.75$ and $St = 1.70$), producing relatively smooth modes. However, for the remaining modes, the employment of robust SPOD significantly enhances the smoothness of the modes. Moreover, at high frequencies, such as $St = 4$, the coherent structures extracted with the SPOD technique are not

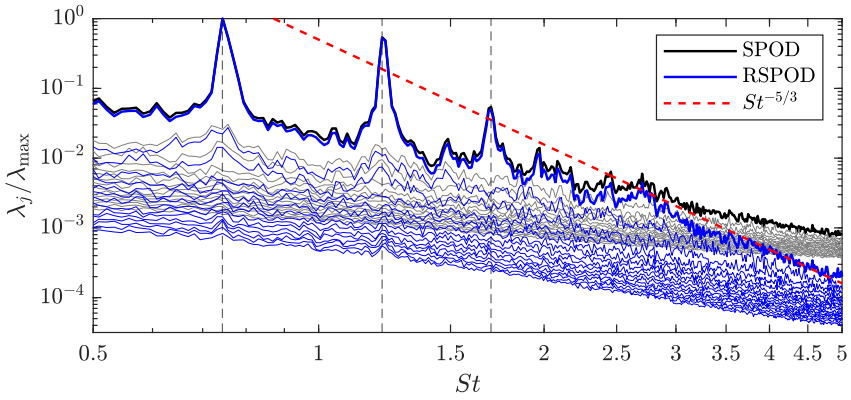

Figure 3: Comparison between the SPOD spectrum (black) and the robust SPOD spectrum (blue) for the cavity flow. The reference red dashed curve represents $St^{-5/3}$. Vertical dashed lines represent Rossiter frequencies.

easily recognizable, whereas the robust SPOD modes exhibit clearer and more distinguishable coherent structures.

To quantify the roughness of the modes, following [36], it is convenient to consider the velocity mode gradient magnitude defined as:

$$\xi_{f_k}(x,y) = \sqrt{\left(\frac{\partial \phi_{u_{f_k}}}{\partial x}\right)^2 + \left(\frac{\partial \phi_{u_{f_k}}}{\partial y}\right)^2 + \left(\frac{\partial \phi_{v_{f_k}}}{\partial x}\right)^2 + \left(\frac{\partial \phi_{v_{f_k}}}{\partial y}\right)^2}, \tag{9}$$

and compute its spatial standard deviation:

$$\sigma_{f_k} = \mathrm{std}(\xi_{f_k}) = \sqrt{\frac{1}{n_x n_y}\sum_{i=1}^{n_x}\sum_{j=1}^{n_y}\left(\xi_{f_k}(x_i,y_j) - \bar{\xi}_{f_k}\right)^2} \tag{10}$$

where $\bar{\xi}_{f_k} = \frac{1}{n_x n_y}\sum_{i=1}^{n_x}\sum_{j=1}^{n_y}\xi_{f_k}(x_i,y_j)$. Figure 5 displays the σ_{f_k} values for the leading four modes obtained from both SPOD and robust SPOD analysis. Comparing the two sets of modes, it is evident that the robust SPOD modes exhibit greater smoothness, particularly at high Strouhal numbers (St). The lower values of σ_{f_k} for robust SPOD modes indicate reduced roughness and enhanced coherence in flow field structures.

4 CONCLUSIONS

This study marks a significant advancement in the analysis of experimental measurements, particularly in contexts where corrupted data and outliers can compromise the accuracy of coherent structure extraction using traditional modal analysis techniques. This challenge is particularly acute at higher frequencies, where noise and uncertainties can severely degrade data quality.

To address these challenges, we introduced a novel approach: robust spectral proper orthogonal decomposition (SPOD), which integrates robust principal component analysis within the SPOD framework. Our investigation centered on assessing this innovative method's effectiveness in enhancing the extraction of coherent structures from complex datasets. The efficacy of robust SPOD was thoroughly evaluated through the analysis of open cavity flow fields obtained from experimental measurements.

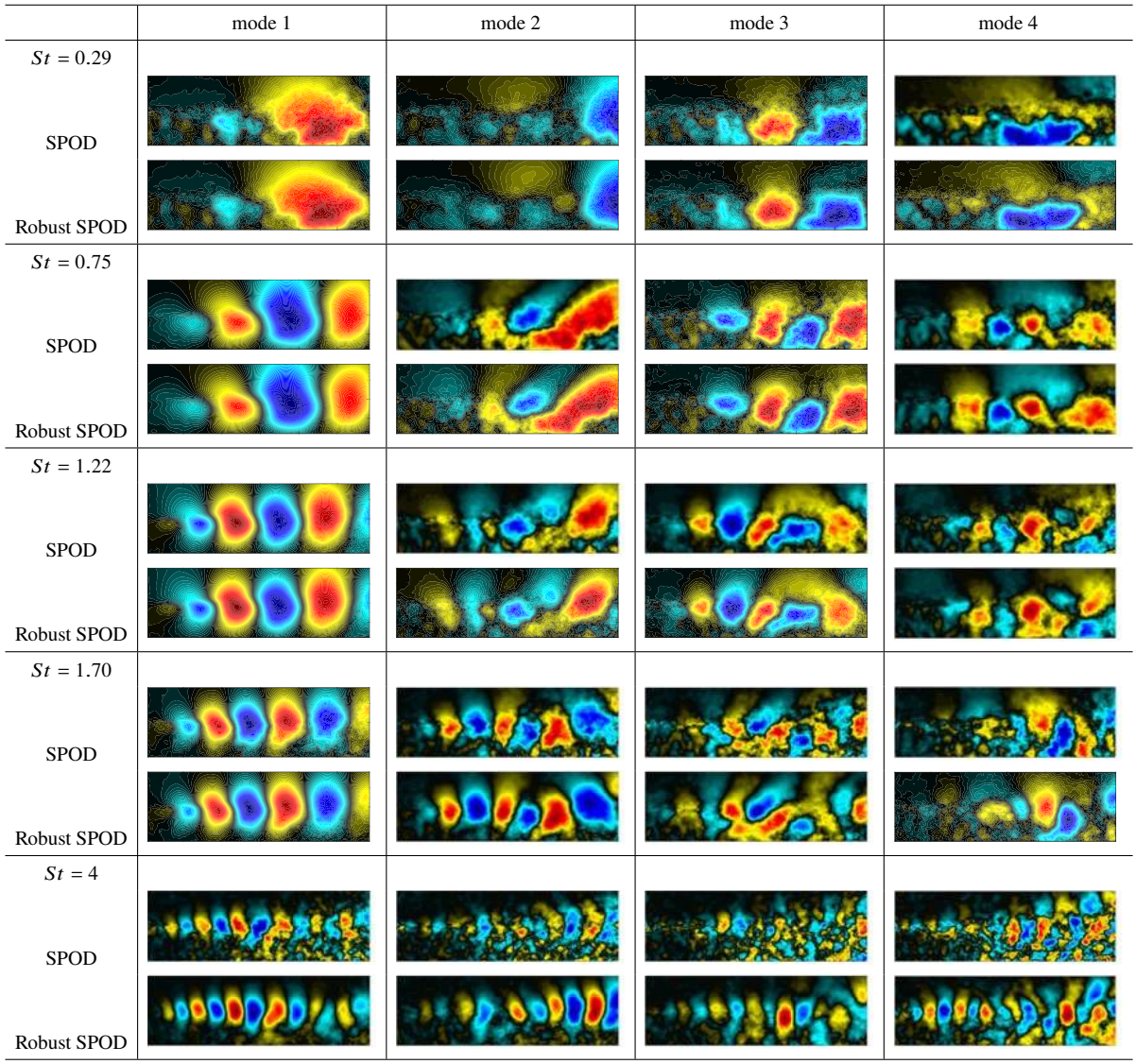

Figure 4: Comparison between SPOD and robust SPOD leading v modes at different St. Field variables have been normalized with respect to their maximum. De-noising parameter $\alpha = 1$. In all panels, the abscissa and ordinate are the dimensionless axial coordinate x/D_c and radial coordinate r/D_c, respectively, omitted for clarity. (blue, cyan, black, yellow, red, $-1 < \phi_{f_k}/\|\phi_{f_k}\|_\infty < 1$. Picture from [32])

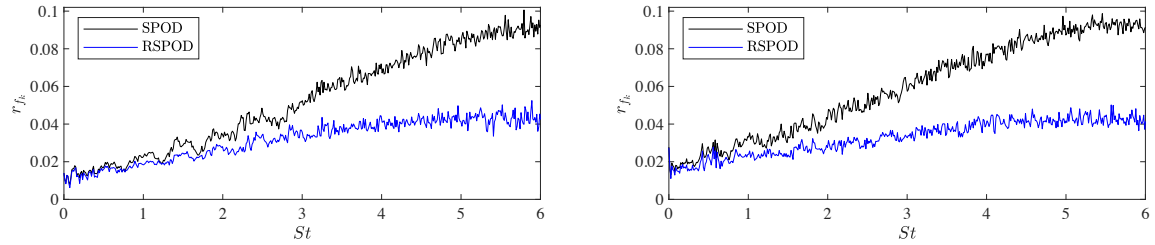

(a) mode 1

(b) mode 2

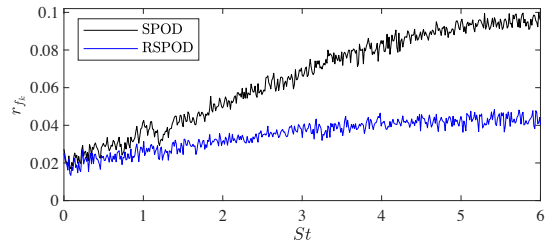

(c) mode 3

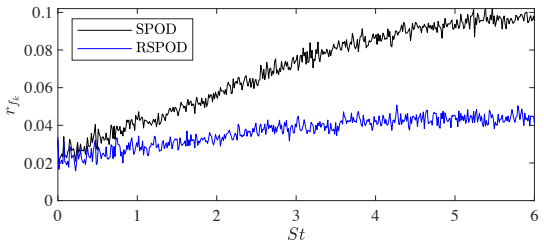

(d) mode 4

Figure 5: Spatial standard deviation of the velocity mode gradient magnitude. Comparison between SPOD and robust SPOD.

The robust SPOD technique demonstrates clear superiority over classical SPOD, particularly at high frequencies, by yielding modes that are both more physically interpretable and better converged. By reconstructing signals from de-noised modes, we demonstrated that robust SPOD effectively mitigates the adverse effects of noise and uncertainties, thereby enhancing data interpretation.

The promising outcomes from both numerical and experimental datasets suggest that robust SPOD has significant potential to deepen our understanding of complex fluid dynamics phenomena and to improve the robustness of modal analysis in various practical applications.

References

[1] Bernd R. Noack, Konstantin Afanasiev, Marek Morzyński, Gilead Tadmor, and Frank Thiele. A hierarchy of low-dimensional models for the transient and post-transient cylinder wake. *Journal of Fluid Mechanics*, 497:335–363, 2003.

[2] C.W. Rowley and S.T.M. Dawson. Model reduction for flow analysis and control. *Annual Review of Fluid Mechanics*, 49:387–417, 2017.

[3] K. Taira, S.L. Brunton, S.T.M. Dawson, C.W. Rowley, T. Colonius, B.J. McKeon, O.T. Schmidt, S. Gordeyev, V. Theofilis, and L.S. Ukeiley. Modal analysis of fluid flows: An overview. *AIAA Journal*, 55(12):4013–4041, 2017.

[4] O. Schmidt, A. Towne, G. Rigas, T. Colonius, and G. Brès. Spectral analysis of jet turbulence. *Journal of Fluid Mechanics*, 855, 11 2018.

[5] A. Towne, O. T. Schmidt, and T. Colonius. Spectral proper orthogonal decomposition and its relationship to dynamic mode decomposition and resolvent analysis. *Journal of Fluid Mechanics*, 847:821–867, 2018.

[6] Oliver T. Schmidt. Spectral proper orthogonal decomposition using multitaper estimates. *Theoretical and Computational Fluid Dynamics*, 36(5):741–754, August 2022.

[7] M. Chiatto, J. K. Shang, L. de Luca, and F. Grasso. Insights into low reynolds flow past finite curved cylinders. *Physics of Fluids*, 33(3):035150, 2021.

[8] Matteo Chiatto, Caroline Cardinale, Jessica K. Shang, and Francesco Grasso. Analysis of the wake flow behind concave curved cylinders with velocity measurements by particle image velocimetry and modal decomposition. *Physics of Fluids*, 35(7), 2023.

[9] A. Colanera, A. Della Pia, M. Chiatto, L. de Luca, and F. Grasso. Modal decomposition analysis of unsteady viscous liquid sheet flows. *Physics of Fluids*, 33(9):092117, 2021.

[10] S. Nidhan, K. Chongsiripinyo, O. T. Schmidt, and S. Sarkar. Spectral proper orthogonal decomposition analysis of the turbulent wake of a disk at re = 50 000. *Phys. Rev. Fluids*, 5:124606, Dec 2020.

[11] Leandra I. Abreu, André V. G. Cavalieri, Philipp Schlatter, Ricardo Vinuesa, and Dan S. Henningson. Spectral proper orthogonal decomposition and resolvent analysis of near-wall coherent structures in turbulent pipe flows. *Journal of Fluid Mechanics*, 2020.

[12] M. Chiatto, L. de Luca, and F. Grasso. Modal analysis of actively controlled flow past a backward facing ramp. *Physical review fluids*, 6:064608, 2021.

[13] H. Huang, D. Dabiri, and M. Gharib. On errors of digital particle image velocimetry. *Measurement Science and Technology*, 8(12):1427 – 1440, 1997.

[14] Jerry Westerweel and Fulvio Scarano. Universal outlier detection for piv data. *Experiments in Fluids*, 39(6):1096 – 1100, 2005.

[15] M.A. Oliver and R. Webster. Kriging: A method of interpolation for geographical information systems. *International Journal of Geographical Information Systems*, 4(3):313 – 332, 1990.

[16] Richard M. Everson and Lawrence Sirovich. Karhunen–loève procedure for gappy data. *Journal of The Optical Society of America A-optics Image Science and Vision*, 12:1657–1664, 1995.

[17] Daniele Venturi and George Karniadakis. Gappy data and reconstruction procedures for flow past a cylinder. *Journal of Fluid Mechanics*, 519:315–336, 2004.

[18] Hasan Gunes, Sirod Sirisup, and George Karniadakis. Gappy data: To krig or not to krig? *Journal of Computational Physics*, 212(1):358–382, 2006.

[19] Akhil Nekkanti and Oliver T. Schmidt. Gappy spectral proper orthogonal decomposition. *Journal of Computational Physics*, 478:111950, 2023.

[20] Jakob G. R. Von Saldern, Johann Moritz Reumschüssel, Thomas L. Kaiser, Moritz Sieber, and Kilian Oberleithner. Mean flow data assimilation based on physics-informed neural networks. *Physics of Fluids*, 34(11), 2022.

[21] Elise Özalp, Georgios Margazoglou, and Luca Magri. Reconstruction, forecasting, and stability of chaotic dynamics from partial data. *Chaos: An Interdisciplinary Journal of Nonlinear Science*, 33(9), September 2023.

[22] M. Buzzicotti, F. Bonaccorso, P. Clark Di Leoni, and L. Biferale. Reconstruction of turbulent data with deep generative models for semantic inpainting from turb-rot database. *Physical Review Fluids*, 6(5), 2021.

[23] Stefano Discetti and Yingzheng Liu. Machine learning for flow field measurements: a perspective. *Measurement Science and Technology*, 34(2), 2023.

[24] E. Candes, X. Li, Y. Ma, and J. Wright. Robust principal component analysis? *Journal of the ACM*, 58, 12 2009.

[25] X. Yuan and J. Yang. Sparse and low rank matrix decomposition via alternating direction method. *Pacific Journal of Optimization*, 9, 01 2009.

[26] Z. Lin, M. Chen, and Y. Ma. The augmented lagrange multiplier method for exact recovery of corrupted low-rank matrices. *Mathematical Programming*, 9, 09 2010.

[27] I. Scherl, B. Strom, J. Shang, O. Williams, B. Polagye, and S. Brunton. Robust principal component analysis for modal decomposition of corrupt fluid flows. *Physical Review Fluids*, 5, 05 2020.

[28] Sirovich Lawrence. Turbulence and the dynamics of coherent structures. i. coherent structures. *Quarterly of Applied Mathematics*, 45:561–571, 1987.

[29] Yang Zhang, Yiyang Sun, Nishul Arora, Louis N. Cattafesta III, Kunihiko Taira, and Lawrence S. Ukeiley. Suppression of cavity flow oscillations via three-dimensional steady blowing. *AIAA Journal*, 57(1):90–105, 2019.

[30] O. T. Schmidt and T. Colonius. Guide to spectral proper orthogonal decomposition. *AIAA Journal*, 58(3):1023–1033, 2020.

[31] A. Colanera, A. Della Pia, and M. Chiatto. Data-driven global stability of vertical planar liquid jets by dynamic mode decomposition on random perturbations. *Physics of Fluids*, 34, 12 2022.

[32] Antonio Colanera, Oliver T. Schmidt, and Matteo Chiatto. Robust spectral proper orthogonal decomposition. *Submitted to Computer Physics Communications*, 2024, doi: 10.2139/ssrn.4899112.

[33] Yiyang Sun, Kunihiko Taira, Louis N. Cattafesta, and Lawrence S. Ukeiley. Biglobal instabilities of compressible open-cavity flows. *Journal of Fluid Mechanics*, 826:270–301, 2017.

[34] Yiyang Sun, Qiong Liu, Louis N. Cattafesta, Lawrence S. Ukeiley, and Kunihiko Taira. Resolvent analysis of compressible laminar and turbulent cavity flows. *AIAA Journal*, 58(3):1046 – 1055, 2020.

[35] J.E. Rossiter. *Wind tunnel experiments on the flow over rectangular cavities at subsonic and transonic speeds*. Number 3438 in ARC 26621. Ministry of Aviation, 1964.

[36] Carlos Henrique Grohmann, Mike J. Smith, and Claudio Riccomini. Multiscale analysis of topographic surface roughness in the midland valley, scotland. *IEEE Transactions on Geoscience and Remote Sensing*, 49(4):1200 – 1213, 2011.